Quantum Fields on Discrete Proper Time: Vacuum Stress–Energy Corrections, Non-Equilibrium Phenomenology, and Experimental Targets

Julio C. Spinelli
Independent Researcher
(Dated: September 23, 2025)

Context: This work builds on our discrete proper-time framework (Spinelli, engrXiv DOI:10.31224/5376), where proper time is discretized at the Planck scale, yielding a finite Lorentz factor and a modified dispersion relation (MDR). Here we develop its quantum-vacuum and phenomenological consequences. Rather than rederiving those results, we (i) embed the MDR in a minimal quantum field theory (QFT) and check microcausality/unitarity to leading order; (ii) introduce a covariant *desynchronization tensor* $\Delta_{\mu\nu}$ that quantifies phase mismatches between proper-time slices and compute its leading contribution to the renormalized stress–energy tensor $\langle T_{\mu\nu}\rangle$; (iii) derive analytic, Planck-suppressed corrections to Casimir energies and photon group velocities; and (iv) formulate conservative, falsifiable experimental targets for optical resonators, dynamical Casimir platforms, and astrophysical time-of-flight. All results are consistent with precision Lorentz tests. We frame any "vacuum pumping" strictly as non-equilibrium QFT requiring external work, with backreaction and entropy production accounted for.

Keywords: discrete time, Lorentz invariance, modified dispersion, Casimir effect, quantum vacuum

I. INTRODUCTION AND SCOPE

This paper extends the discrete proper-time (DPT) framework introduced in Ref. [1] toward vacuum-energy corrections and phenomenology. Discretizing proper time at $t_{\rm P}$ modifies relativistic kinematics while remaining local along worldlines, leading to the modified dispersion relation (MDR)

$$\frac{4\hbar^2}{t_{\rm P}^2}\,\sin^2\!\Big(\frac{E\,t_{\rm P}}{2\hbar}\Big) = p^2c^2 + m^2c^4, \tag{1}$$

which saturates energies at $\pi\hbar/t_{\rm P}$ and regularizes the Lorentz factor at ultra-high energy. Here we develop a nonredundant extension: a QFT embedding with microcausality/unitarity checks, a stochastic covariant description of inter-slice phase mismatches ("desynchronization"), and explicit, testable predictions for laboratory and astrophysical observables, contrasted to bounds from Lorentz-invariance tests [2–5].

Related engineering-facing preprints on engrXiv illustrate how experimental platforms are evolving in directions relevant to our proposals. For example, Lally [6] explores MEMS-based nanofabrication techniques aimed at precision Casimir measurements, while Ram [7] surveys cryocooler conduction approaches for superconducting resonator systems. These developments highlight practical routes toward realizing the non-equilibrium cavity and metrology experiments we outline below.

II. MINIMAL QFT ON DISCRETE PROPER TIME

a. Reproducibility note. All figures in this work (Figs. 3–4) are generated from the analytic expressions using the companion Jupyter notebook included as a supplementary galley. The code requires only `numpy`, `scipy`, and `matplotlib` and reproduces all plots as shown. Quantization proceeds as usual with $[\hat{a}_{\boldsymbol{p}}, \hat{a}^\dagger_{\boldsymbol{p}'}] = \delta^{(3)}(\boldsymbol{p}-\boldsymbol{p}')$; the novelty is the mode frequency from (1). The small-$t_{\rm P}$ expansion yields

$$E(\boldsymbol{p}) \simeq E_0(\boldsymbol{p})\Big[1 + \frac{E_0^2(\boldsymbol{p})}{24E_{\rm P}^2}\Big],\; E_0 = \sqrt{p^2c^2+m^2c^4}, \tag{2}$$

with $E_{\rm P} = \hbar/t_{\rm P}$. The Pauli–Jordan function receives $\mathcal{O}(E^2/E_{\rm P}^2)$ corrections that vanish outside the usual light cone at this order, so perturbative microcausality is preserved.[1] For photons ($m=0$),

$$v_g = \frac{\partial E}{\partial p} \simeq c\Big[1 + \frac{E^2}{8E_{\rm P}^2}\Big] + \mathcal{O}(E^4/E_{\rm P}^4). \tag{3}$$

Here $E_{\rm P} = \hbar/t_{\rm P}$ and Eq. (3) holds in the low-energy regime $E \ll E_{\rm P}$ for narrowband wave packets where group velocity is meaningful. Signal fronts remain luminal, so no superluminal signaling is implied [3]. Throughout, we therefore emphasize observable time-of-flight and resonator consequences rather than raw v_g offsets.

III. DESYNCHRONIZATION TENSOR AND STRESS–ENERGY

We model stochastic phase mismatches among proper-time ticks by a symmetric, dimensionless $\Delta_{\mu\nu}(x)$ with zero mean and two-point function $\langle \Delta_{\mu\nu}(x)\Delta_{\rho\sigma}(y)\rangle = \sigma_\Delta^2\,\mathcal{K}_{\mu\nu\rho\sigma}(x-y)$. To leading order in $t_{\rm P}$ and Δ, point-splitting renormalization for a free field gives

$$\delta\langle T_{\mu\nu}\rangle \simeq \chi\,\sigma_\Delta^2\,\frac{\hbar}{t_{\rm P}^2}\Big(\ell_{\rm corr}^2\nabla_\mu\nabla_\nu - \tfrac{1}{4}\eta_{\mu\nu}\ell_{\rm corr}^2\Box\Big)\langle\phi^2\rangle_{\rm ren}, \tag{4}$$

[1] Signal fronts remain luminal; group velocities may receive Planck-suppressed advances without enabling superluminal signaling [3].

where $\ell_{\rm corr}$ is the correlation length and χ is a dimensionless coefficient fixed by the field content, and $\Box \equiv \frac{\partial^2}{\partial t^2} - \frac{\partial^2}{\partial x^2} - \frac{\partial^2}{\partial y^2} - \frac{\partial^2}{\partial z^2}$ denotes the d'Alembert (wave) operator. Equation (4) provides a covariant handle on anisotropic vacuum-pressure corrections sourced by desynchronization.

IV. CASIMIR ENERGY WITH DISCRETE TIME

For parallel perfect conductors separated by a, the standard result is $E_0/A = -\pi^2\hbar c/(720a^3)$ [8, 9]. With the photon MDR (2), each mode frequency shifts by $\delta\omega/\omega \simeq (\hbar\omega)^2/(24E_{\rm P}^2)$, yielding

$$\frac{\delta E}{E_0} \simeq \frac{\pi^2}{24}\left(\frac{\ell_{\rm P}}{a}\right)^2, \qquad \frac{\delta F}{F_0} \simeq \frac{5\pi^2}{24}\left(\frac{\ell_{\rm P}}{a}\right)^2, \tag{5}$$

with $\ell_{\rm P} = c\,t_{\rm P}$. At $a = 100\,\text{nm}$ this is $\sim 10^{-52}$, implying equilibrium Casimir experiments cannot probe the MDR directly; non-equilibrium probes are required.

V. PHENOMENOLOGY AND EXPERIMENTAL TARGETS

A. Astrophysical time-of-flight

From (3), a photon of energy E over distance L accumulates $\Delta t \simeq -(L/c)\,E^2/(8E_{\rm P}^2)$. Fermi GRB constraints on quadratic Lorentz violation [2, 3, 10] are consistent with this scaling.

B. Optical resonators and clocks

Fractional shifts follow $\delta\nu/\nu \sim (h\nu)^2/(24E_{\rm P}^2)$ for the free photon; anisotropic $\Delta_{\mu\nu}$ induces SME-like signatures [4]. We propose rotating, cryogenic, ultra-high-Q cavities monitored by dual frequency combs to bound σ_Δ at the 10^{-15}–10^{-18} fractional level, limited by thermal/technical noise.

C. Driven, non-equilibrium platforms

Dynamical Casimir (DCE) systems [9, 11–13] provide controlled boundary modulation. In our framework, coherent modulation sources $\Delta_{\mu\nu}(t)$; Eq. (4) predicts a small, phase-tunable anisotropic pressure. Any net output is accounted for by the external pump (no violation of the second law); backreaction renormalizes the effective pump impedance.

Curved-spacetime estimate inside laboratory cavities. The curved-covariant extension in App. C [Eq. (C1)] shows that $\delta\langle T_{\mu\nu}\rangle$ splits into a flat-space, local differential piece $A\,\mathcal{D}_{\mu\nu}[f]$ plus curvature-suppressed counterterms

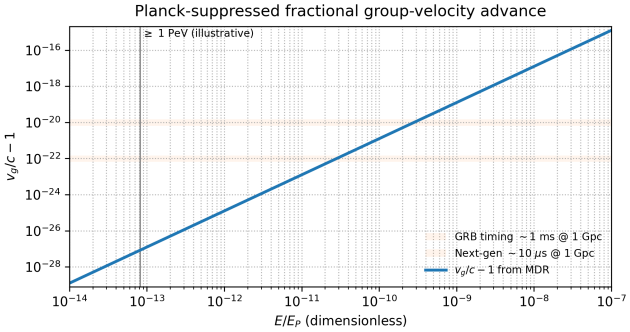

FIG. 1. Fractional group-velocity advance $(v_g/c-1)$ versus the dimensionless ratio $E/E_{\rm P}$ using the leading-order MDR scaling $(v_g/c-1) \simeq (E/E_{\rm P})^2/8$.
The focused range makes the quadratic Planck suppression explicit.
Faint horizontal bands indicate illustrative short-GRB timing sensitivities mapped via $(v_g/c-1) \lesssim c\,\Delta t/L$ (examples: 1 ms and 10 μs at $L \sim 1$ Gpc).
A thin vertical line marks $E = 1$ PeV to contextualize current observations. Observable consequences are developed via time-of-flight in Fig. 2.

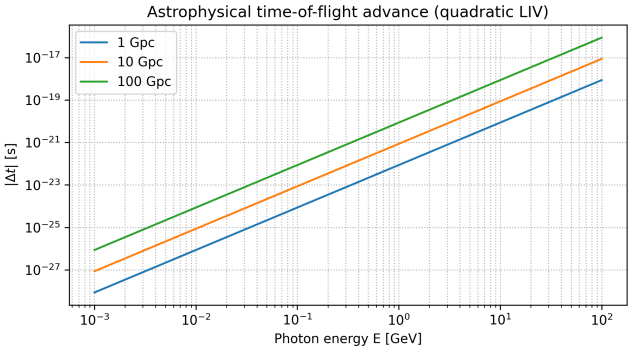

FIG. 2. Astrophysical time-of-flight advance Δt vs. photon energy E for representative distances $L = \{1, 10, 100\}$ Gpc using Eq. (3).

proportional to $G_{\mu\nu}f$, $H^{(1)}_{\mu\nu}f$, and $H^{(2)}_{\mu\nu}f$, each weighted by $\mathcal{O}(\ell^2_{\rm corr})$ coefficients. For a terrestrial superconducting resonator of linear size $L \sim 0.1$–$1\,\text{m}$ one has $\ell_{\rm corr} \lesssim L$ while the background curvature radius $\mathcal{R}^{-1/2}$ associated with Earth's weak field is astronomically larger; hence $\ell^2_{\rm corr}/\mathcal{R}^{-1} \ll 1$, and the curvature terms in Eq. (C1) are utterly negligible compared to the flat contribution $A\,\mathcal{D}_{\mu\nu}[f]$. Operationally, cavity experiments can therefore analyze signals using the flat-space prediction (Sec. V) and treat curvature pieces as a systematic bounded by $\propto (\ell_{\rm corr}/\mathcal{R}^{-1/2})^2\,|f|$. In space-based or strong-field platforms the same scaling provides a conservative upper bound; curvature corrections remain subleading unless $\ell_{\rm corr}$ approaches the local curvature radius. See Fig. 4 for representative scaling.

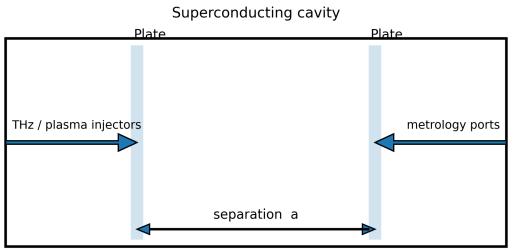

FIG. 3. Schematic non-equilibrium platform: a superconducting cavity with two parallel plates defines the inter-plate region (shaded bars). THz/plasma injectors drive non-adiabatic boundary conditions; metrology ports are located outside the inter-plate region for force/phase readout.

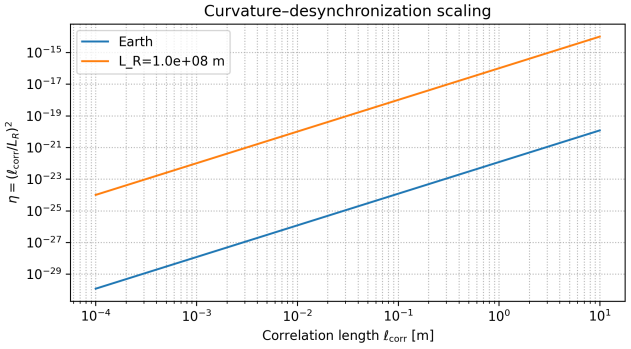

FIG. 4. Curvature–desynchronization figure of merit $\eta = (\ell_{\rm corr}/L_R)^2$ vs. correlation length $\ell_{\rm corr}$ for Earth and a stronger-curvature example. Terrestrial platforms lie deep in the $\eta \ll 1$ regime.

VI. CONCLUSIONS

This preprint extends the discrete proper-time framework of Spinelli (engrXiv DOI:10.31224/5376) into vacuum-energy and phenomenology. A forthcoming manuscript addresses the interpretational program—gravity as re/synchronization—and consolidates experimental targets. Together these form a coherent three-part series: (i) kinematics and MDR, (ii) vacuum-energy and stress–tensor phenomenology (this paper), and (iii) gravitational reinterpretation. The discrete proper-time MDR leads to even-powered, Planck-suppressed kinematics compatible with precision tests. The desynchronization tensor provides a covariant, falsifiable parameterization of possible inter-slice correlations, with concrete laboratory strategies in non-equilibrium platforms. From an engineering perspective, these strategies overlap with preprint-stage developments in MEMS/Casimir metrology [6] and cryogenic superconducting cavities [7], providing natural experimental interfaces for the framework. Future work includes curved backgrounds, multi-field sectors, and lattice worldline numerics to compute the coefficient χ and kernels $\mathcal{K}_{\mu\nu\rho\sigma}$.

TABLE I. Order-of-magnitude targets and present bounds.

Observable	Scaling	Status/Target
$v_g/c-1$	$+E^2/(8E_{\rm P}^2)$	Consistent with GRB bounds [10]
Casimir $\delta F/F_0$	$\frac{5\pi^2}{24}(\ell_{\rm P}/a)^2$	$\sim 10^{-52}$ at $a = 100\,$nm
Optical $\delta\nu/\nu$	$(\hbar\nu)^2/(24E_{\rm P}^2)$	Target 10^{-18} fractional
$\delta\langle T_{\mu\nu}\rangle$	$\propto \sigma_\Delta^2 \ell_{\rm corr}^2$	DCE force metrology

Note. Curvature-suppressed contributions (App. C) are negligible in terrestrial cavities when $\eta = (\ell_{\rm corr}/L_R)^2 \ll 1$; see Fig. 4.

This article forms the second part of a sequence of preprints on discrete proper time. The first installment established the finite Lorentz factor and MDR framework [1], while the present work develops its consequences for vacuum stress–energy, Casimir phenomenology, and non-equilibrium platforms. A forthcoming manuscript will extend the program to gravitational reinterpretation in terms of re/synchronization, completing a coherent three-part research arc.

ACKNOWLEDGMENTS

The author thanks colleagues for discussions on cavity QED, DCE, and frequency-comb metrology. This article builds on the discrete proper-time proposal of Ref. [1].

Appendix A: Derivation of Eqs. (3) and (5)

Group velocity

From (1) with $m = 0$, $E = \frac{2\hbar}{t_{\rm P}} \arcsin\!\left(\frac{pc\,t_{\rm P}}{2\hbar}\right)$. Expanding for $pc \ll E_{\rm P}$ gives $E \simeq pc\left[1 + \frac{(pc)^2}{24E_{\rm P}^2}\right]$ and $v_g = \partial E/\partial p \simeq c\left[1 + \frac{E^2}{8E_{\rm P}^2}\right]$.

Casimir shift

Mode frequencies shift as $\delta\omega/\omega \simeq (\hbar\omega)^2/(24E_{\rm P}^2)$. Using the standard mode-sum with zeta regularization, the renormalized energy scales as ω^1; thus $\delta E/E_0 = \langle\delta\omega/\omega\rangle = \frac{1}{24E_{\rm P}^2}\langle(\hbar\omega)^2\rangle$. Evaluating the average on the plate spectrum yields Eq. (5).

Appendix B: Microcausality to leading order

Expanding the Pauli–Jordan function with the deformed $\omega(\boldsymbol{p})$ shows that the $\mathcal{O}(E^2/E_{\rm P}^2)$ term integrates to

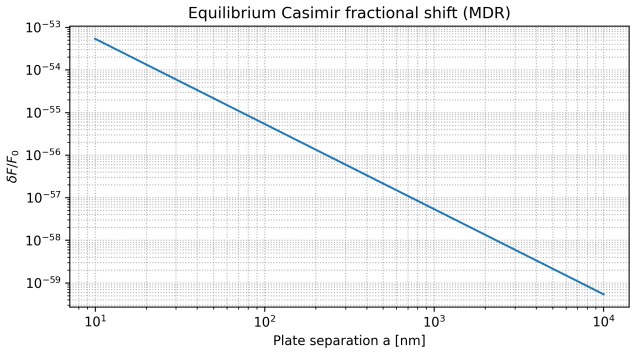

FIG. 5. Fractional Casimir-force shift $\delta F/F_0$ versus plate separation a from the MDR scaling, $\delta F/F_0 \propto (\ell_{\rm P}/a)^2$. The effect is far below present equilibrium sensitivity across $a \in [10\,\mathrm{nm}, 10\,\mu\mathrm{m}]$, motivating non-equilibrium probes.

a derivative of the standard light-cone distribution; support remains on the cone to this order. Front velocities remain luminal [3].

Appendix C: Curved-spacetime covariantization of $\delta\langle T_{\mu\nu}\rangle$

We now promote the flat-space expression in Eq. (4) to a curved background $(\mathcal{M}, g_{\mu\nu})$. Let $f(x) \equiv \langle\phi^2(x)\rangle_{\rm ren}$ be the renormalized scalar composite in the Hadamard scheme [14–16]. Assume the desynchronization statistics are homogeneous over scales large compared with the microscopic correlation length $\ell_{\rm corr}$ and small compared with the background curvature radius $\mathcal{R}^{-1/2}$ (adiabatic order two). To leading order in σ_Δ and $\ell_{\rm corr}$, general covariance and locality restrict the correction to the renormalized stress–energy tensor to the form

$$\delta\langle T_{\mu\nu}\rangle \simeq \chi\,\sigma_\Delta^2\,\frac{\hbar}{t_{\rm P}^2}\left(\ell_{\rm corr}^2\nabla_\mu\nabla_\nu - \tfrac{1}{4}\eta_{\mu\nu}\ell_{\rm corr}^2\Box\right)\langle\phi^2\rangle_{\rm ren}, \tag{C1}$$

where $A \equiv \chi\,\sigma_\Delta^2\,(\hbar/t_{\rm P}^2)\,\ell_{\rm corr}^2$ and the second line collects curvature–suppressed, state–dependent counterterms permitted by covariance and dimensional analysis. The minimal covariant differential operator is chosen as

$$\mathcal{D}_{\mu\nu}[f] \;\equiv\; \nabla_\mu\nabla_\nu f - \frac{1}{4}g_{\mu\nu}\Box f + \xi_c\left(R_{\mu\nu} - \tfrac{1}{4}g_{\mu\nu}R\right)f, \tag{C2}$$

with ξ_c a dimensionless constant. For a conformally coupled massless scalar, $\xi_c = \frac{1}{6}$ reproduces the known structure of curvature contributions to composite operators [14, 15].

The tensors $H_{\mu\nu}^{(1)}$ and $H_{\mu\nu}^{(2)}$ are the standard local geometric variations [14, 16]:

$$H_{\mu\nu}^{(1)} \equiv 2\nabla_\mu\nabla_\nu R - 2g_{\mu\nu}\Box R - \tfrac{1}{2}g_{\mu\nu}R^2 + 2RR_{\mu\nu}, \tag{C3}$$

$$H_{\mu\nu}^{(2)} \equiv 2\nabla_\alpha\nabla_{(\mu}R_{\nu)}{}^{\alpha} - \Box R_{\mu\nu} - \tfrac{1}{2}g_{\mu\nu}\Box R - \tfrac{1}{2}g_{\mu\nu}R_{\alpha\beta}R^{\alpha\beta} + 2R_{\mu\alpha\nu\beta}R^{\alpha\beta}, \tag{C4}$$

and $G_{\mu\nu}$ is the Einstein tensor.

Conservation. Because desynchronization is driven by an external (pump) sector that exchanges energy–momentum with the field, $\delta\langle T_{\mu\nu}\rangle$ need not be separately conserved. The semiclassical Bianchi identity is enforced at the level of the full system:

$$\nabla^\mu\Big(\langle T_{\mu\nu}\rangle_{\rm ren} + \delta\langle T_{\mu\nu}\rangle + T_{\mu\nu}^{\rm pump}\Big) = 0. \tag{C5}$$

In the absence of driving (stationary stochastic $\Delta_{\mu\nu}$ with covariantly constant two-point kernel) and to adiabatic order two, one can absorb the residual $\nabla^\mu\delta\langle T_{\mu\nu}\rangle$ into the curvature counterterms of Eq. (C1) by an appropriate choice of $(\xi_c, \alpha_1, \alpha_2, \alpha_3)$, consistent with Hadamard renormalization freedom [14, 15]. Explicitly, using the commutator $[\nabla_\mu, \nabla_\nu]\nabla_\alpha f = R_{\mu\nu\alpha}{}^{\beta}\nabla_\beta f$ and the contracted Bianchi identity $\nabla^\mu G_{\mu\nu} = 0$, the divergence of $\mathcal{D}_{\mu\nu}[f]$ is curvature-suppressed, $\nabla^\mu\mathcal{D}_{\mu\nu}[f] = \mathcal{O}(R\nabla f)$, and can be cancelled to this order by the curvature terms in (C1).

Semiclassical coupling. In curved spacetime the correction enters the semiclassical Einstein equations as

$$G_{\mu\nu} + \Lambda g_{\mu\nu} = 8\pi G\Big(\langle T_{\mu\nu}\rangle_{\rm ren} + \delta\langle T_{\mu\nu}\rangle\Big), \tag{C6}$$

with $\delta\langle T_{\mu\nu}\rangle$ given by (C1). Inside non-equilibrium cavities (Sec. V), Eq. (C1) predicts a tiny, anisotropic vacuum pressure proportional to A and controlled by the external modulation through f.

Domain of validity. Equation (C1) holds provided $\ell_{\rm corr} \ll \mathcal{R}^{-1/2}$ and gradients are small on that scale. Higher-derivative and nonlocal tails enter at $\mathcal{O}(\ell_{\rm corr}^4)$ and can be organized by the Schwinger–DeWitt/adiabatic expansion [14, 15].

DATA AND CODE AVAILABILITY

The Python/Jupyter notebook used to generate Figs. 3–4 and to reproduce the order-of-magnitude estimates is provided as ancillary material; running it regenerates all figures with documented parameter choices.

[1] J. C. Spinelli, Finite lorentz factor from discrete proper-time quantization: modified dispersion relation and phenomenology (2025), preprint.

[2] D. Mattingly, Living Reviews in Relativity **8**, 10.12942/lrr-2005-5 (2005).

[3] S. Liberati, Classical and Quantum Gravity **30**, 133001 (2013).
[4] V. A. Kostelecký, Physical Review D **69**, 105009 (2004).
[5] S. Hossenfelder, Living Reviews in Relativity **16**, 10.12942/lrr-2013-2 (2013).
[6] R. Lally, The construction of a fully integrated, mems based, micro-nanofabrication facility for the development of extreme low temperature devices (2021), applications include Casimir searches.
[7] D. Ram, Comparison of copper and aluminum as the thermal link material in cryocooler conduction cooled srf cavities (2022), cryocooler conduction to superconducting RF cavities.
[8] H. B. G. Casimir, Proc. K. Ned. Akad. Wet. **51**, 793 (1948).
[9] K. A. Milton, *The Casimir Effect: Physical Manifestations of Zero-Point Energy* (World Scientific, Singapore, 2001).
[10] A. A. A. et al., Science **323**, 1688 (2009).
[11] G. T. Moore, Journal of Mathematical Physics **11**, 2679 (1970).
[12] P. D. Nation, J. R. Johansson, M. P. Blencowe, and F. Nori, Rev. Mod. Phys. **84**, 1 (2012).
[13] C. M. Wilson, G. Johansson, A. Pourkabirian, M. Simoen, J. R. Johansson, T. Duty, F. Nori, and P. Delsing, Nature **479**, 376 (2011).
[14] N. D. Birrell and P. C. W. Davies, *Quantum Fields in Curved Space* (Cambridge University Press, Cambridge, 1982).
[15] R. M. Wald, *Quantum Field Theory in Curved Spacetime and Black Hole Thermodynamics* (University of Chicago Press, Chicago, 1994).
[16] S. M. Christensen, Phys. Rev. D **14**, 2490 (1976).